Int. J. Electrochem. Sci., 9 **(2014)** 4478 - 4492

International Journal of
ELECTROCHEMICAL
SCIENCE
www.electrochemsci.org

$Ni_{0.5}Zn_{0.5}Fe_2O_4$ as a Potential Corrosion Inhibitor for API 5L X80 Steel in Acidic Environment

A.U. Chaudhry[1,*], *Rahul Bhola*[1], *Vikas Mittal*[2], *Brajendra Mishra*[1]

[1]Department of Metallurgical & Materials Engineering, Colorado School of Mines, CO. 80401, USA.
[2]Department of Chemical Engineering, The Petroleum Institute, Abu Dhabi, P.O. Box 2533, UAE.
[*]E-mail: cusman@mines.edu

Received: 25 February 2014 / *Accepted:* 22 April 2014 / *Published:* 19 May 2014

Corrosion inhibitors are widely used in acid solutions during pickling, cleaning/descaling of boilers and several other industrial applications. Mostly the organic compounds containing N, O and S are employed; however they are high toxic and environmentally non-friendly. In this study, the inhibition performance of nano-powder of ferrites of Ni, Zn and Fe in varying concentrations of 1M sulphuric acid on the corrosion behavior of API 5L X80 steel has been investigated. The nano-powder has been characterized using TEM, FESEM, XRD and its corrosion behavior in 1M H_2SO_4 has been studied using various advanced electrochemical tools such as EIS and potentiodynamic polarization (PD). It has been found that under the given acidic conditions, ferrites act as efficient corrosion inhibitors of steel. The order of inhibition effcencies of ferrite concentrations is 0.008 > 0.01 > 0.05 > 0.07 > 1M sulphuric acid. This inhibition is considerable and can be of significant importance for the oil and gas industry.

Keywords: Corrosion, nano-particles, ferrites, $Ni_{0.5}Zn_{0.5}Fe_2O_4$,sulphuric acid, API 5L X80 Steel, EIS, polarization

1. INTRODUCTION

The addition of corrosion inhibitors to prevent acid induced corrosion is a common and established practice in several industrial systems (especially oil and gas industry). Acid pickling is a phenomenon in which strong acids such as hydrochloric, hydrofluoric, sulphuric, phosphoric and nitric acid are used to leach out impurities from various alloys of iron, copper and aluminum. Moreover, pickling corrodes the containing vessel and is not advantageous to the industrial processes. To prevent such a corrosive attack to the containing environment, inhibitors are added to the acid solution. Mostly organic molecules are used [1], however, researchers have also used vitamins [2] and

other environmentally safe green organic compounds as inhibitors [3]. It has also been reported by several researchers that the use of inorganic inhibitors in acidic environments could be even more detrimental, owing to the severe localized attack once the passive film over the metal is broken [4, 5].

Recent research has shown that spinel based inorganic pigments of the general formula AB_2O_4 have not only distinctive thermal and weather degradation resistance, but are also more environment friendly [6, 7]. These are produced by a combination of two or more cations in the lattice structure and their properties are primarily determined through their lattice characteristics. These type of pigments not only enhance the mechanical strength of the binder but also decrease its permeability towards destructive species [8]. The principle reaction involving the formation of ferrites is given below –

$$MeO + Fe_2O_3 \rightarrow MeFe_2O_4 \qquad -1$$

($MeO.Fe_2O_3$) where Me is Sr, Ba, Mg, Mn, Ni, Zn, or Ca etc.

The general formula for $MeO.Fe_2O_3$ consists of an almost cubic closely packed oxygen arrangement where the cations reside in the tetrahedral and octahedral interstices[9].

The use of spinel based ferrites as pigments in coatings is advantageous owing to their greater anticorrosion efficacy at higher temperatures and aggressive environments [10].

Pigment extract method is a convenient way to know its anticorrosion efficacy on a metal surface and depends upon various factors such as the solubility of pigment in testing solvent, dissolved oxygen concentration, alkalinity of extracts, formation of passive layer, thickness and nature of passive layer, nature of electrolyte, solubility of corrosion products and many more [11, 12].

Pryor et al. [13] used this extract method to study the litharge, metallic lead, red lead, basic lead carbonate, zinc, and zinc oxide in detail. It was further observed that the litharge extracts showed complete corrosion inhibition owing to the formation of α-Fe_2O_3[13]. Similarly, Miszczyk and friends tested the Evan's drop experiment of micronized nickel zinc ferrite extracts in distilled water on steel surface and showed different cathodic and anodic behavior. This phenomenon was referred to the formation of hydroxyl ion due to dissolved oxygen which further reacted with cations present in the extract solution.

These products precipitated on the surface and hindered the electrochemical reaction (equation 2) for the transport of ionic and non-ionic species on the metal surface.

$$yM^{2+} + (3 - y)Fe^{2+} + 6OH^- \rightarrow M_yFe_{(3-y)}(OH)_6 \qquad -2$$

Brodinova et al. [14] also used surface modified ferrites with varying contents of Zn, Mg and Ca cations. The results showed that modified ferrites were better in terms of corrosion protection than the non-modified versions. The corrosion protection mechanism was proposed to be a result of formation of cations soaps which lowered the tendency of the binder to saponify on exposure to the hydroxyl ions formed during corrosion of the metal. Similarly, Wu et al. [15] prepared hybrid coating of PANI layered zinc nickel ferrites and organically modified silicates. The film was deposited via a spin coating on aluminum alloy. The anticorrosion properties of the hybrid film was excellent owing to the denser configuration of organically modified silicate due to the incorporation of nickel zinc ferrites/PANI.

In another work, Kalendová [9] used different types of spinel pigments containing Zn(II), Ca(II), Mg(II), Sr(II), Fe(III), Al(III), and Ti(IV) cations and studied the properties of their extracts. It

was concluded that these ferrites showed varying corrosion inhibition owing to the alkaline nature, solubility of the aqueous phases, and formation of metal soaps and high thermal stability of the spinels.

Furthermore, metals cations also inhibit corrosion in acidic solutions. The charge induced change in the physical and electrical properties of the double layer at the electrolyte-electrode interface directly interferes with the surface adsorption over the metal and thereby prevents corrosion.

Wahdan et al. [16, 17] showed that the maximum protective ability of Cu^{2+} in 1M sulphuric acid was observed at lower concentration. Several researchers also proposed $Zn^{2+,}$ Cd^{2+} and Mn^{2+} to be efficient in acidic solution against corrosion owing to their ability to hinder the hydrogen evaluation reaction [18, 19].

Nano-materials are unique because of their smaller size. The smaller particle has higher surface-to-volume ratio and thus more atoms tend to reside on the surface than inside the particle itself. The use of nano-particles for anticorrosion coatings has achieved significant attention and importance [20]. Several researchers have shown nano particles to perform better and qualify them as a better alternative for anticorrosion coatings in composites and polymers [21].

In the present work, non-toxic, nano particle extracts of nickel zinc ferrites ($Ni_{0.5}Zn_{0.5}Fe_2O_4$) in 1M Sulphuric acid were prepared and their inhibition effects were studied on the API 5L X80 steel.

2. MATERIALS AND METHODS

2.1. Materials Preparation

Nano-powders of $Ni_{0.5}Zn_{0.5}Fe_2O_4$ (99.9% pure, American elements, CA USA) were used as supplied. The impurities details are Al <0.05, Ba <0.05, Ca <0.1, Cd < 0.001, Co <0.05, Cu <0.01, Mg <0.05, Pb <0.001, Si <0.01. API-5L X80 steel coupons having weight percent composition listed as; C 0.07, Mn 1.36, Ti 0.008, S 0.003, P 0.004, Fe Balanced, were machined to 10 × 10 × 4 mm dimensions from a carbon steel pipeline. A tap and drill hole of 3- 48 tpi was drilled to one long side of the coupon. The specimens were finished with different grades of SiC grit papers up to 2400 grit, polished to a mirror finish. The samples were then cleaned and degreased with industrial grade acetone, dried and weighed with an accuracy of ± 1 mg.

The ferrite extracts were prepared according to the method explained by Zin et al [22] A stock solution of the extracts were prepared by solution leaching using 6 gm of each pigment in 1L of 1M H_2SO_4 stirred for 72 hours at room temperature. The solution was filtered using high suction and no residue was found on the filter paper suggesting its complete solubility in 1M H_2SO_4. In order to obtain solutions with different concentrations of nickel zinc ferrites, stock solution was further diluted with 1M H_2SO_4.

2.2. Pigment Characterization

Transmission electron microscopy (TEM) imaging was performed to characterize the nano powder. FEI Philips C200 TEM with point-to-point resolution of 0.11 nm, at 200 kV was used. The

samples were prepared by dispersing approximately 1 mg of NZF in 10 mL of methanol and sonicating for 30 minutes in a water bath at room temperature. One drop of the suspension was then deposited on a 400-mesh copper grid covered with thin amorphous film to view under the microsope.

JEOL JSM-7000F, Field Emission Scanning Electron Microscopy (FE-SEM) was performed to evaluate particle morphology in the nano powder at 2kV under high vaccum at a working distance of 10 mm.

X-ray diffraction (XRD) measurements were performed to determine the crystalline nature of the nano particle. Philips PW 3040/60 spectrometer using Cu Kα radiation in range of 10° to 100° at scan rate 0.050° was used and the peaks and planes obtained were matched using X'Pert HighScore software. Debye–Scherrer equation was further used to confirm the peaks obtained and has been given below (equation 3);

$$\tau = \frac{K\lambda}{\beta cos\Theta} \qquad - 3$$

where, τ is the diameter, β (radian) is the half-intensity width of the relevant diffraction, λ is the x-ray wavelength, K is a dimensionless shape factor (in this case 0.9 was taken) and Θ is the angle of diffraction (in this case is 35 º corresponding to intense peak).

2.3. Electrochemical Measurements

A three-electrode cell assembly consisting of steel coupon as the working electrode (WE), platinum wire as the counter electrode (CE) and a saturated calomel electrode as the reference electrode (RE) was used for the electrochemical measurements. Electrochemical testing was performed in a closed system at room temperature under naturally aerated conditions using a Gamry 600 potentiostat/galvanostat/ZRA. The sequence of electrochemical techniques has been described below.

Electrochemical impedance spectroscopy (EIS): Impedance measurements were performed at the open circuit potential (OCP) at 2 and 5 hours of immersion. The frequency sweep was applied from 10^5 to 10^{-2} Hz with the AC amplitude of 10 mV.

Potentiodynamic polarization: Potentiodynamic polarization measurements were performed at 5 hours of immersion by polarizing the working electrode from an initial potential of -250 mV vs. OCP upto a final potential of 750 mV vs. OCP. A scan rate of 0.1667 mV/s was used for the polarization sweep [23-27].

2.4. Surface Characterization

Surface characterization of the working electrode was performed to carefully evaluate the corrosion products and the metal after the electrochemical attack. Steel coupons were carefully disengaged from the cell assembly, dried and observed under the microscope. The surface film was also gently removed from the coupons and observed under the microscope.

FEI Quanta 600i Environmental Scanning Electron Microscope (ESEM) with PGT Prism Energy Dispersive X-Ray Spectrometer (EDS), X-ray diffraction (XRD) and Bio-Rad Fourier transform infrared spectroscopy (FT-IR) were used to investigate the surface morphology and

elemental composition of the corrosion products. For ESEM the samples were gold coated before use and observed at 20 kV and a working distance of 10 mm . XRD analysis was also performed to differentiate between the various phases present in the corrosion products over the metal coupon. Philips PW 3040/60 spectrometer using Cu Kα radiation in range of 10° to 100° with scan rate of 0.050° was used and the peaks and planes were analyzed using X'Pert HighScore software. FTIR was performed in a range of 400-4000 cm^{-1} at a scan rate of 100 scans/spectrum using the Perkin Elmer model Fourier Transform Infrared. Corroded steel samples were directly placed on the testing plate at room temperature.

3. RESULTS AND DISCUSSION

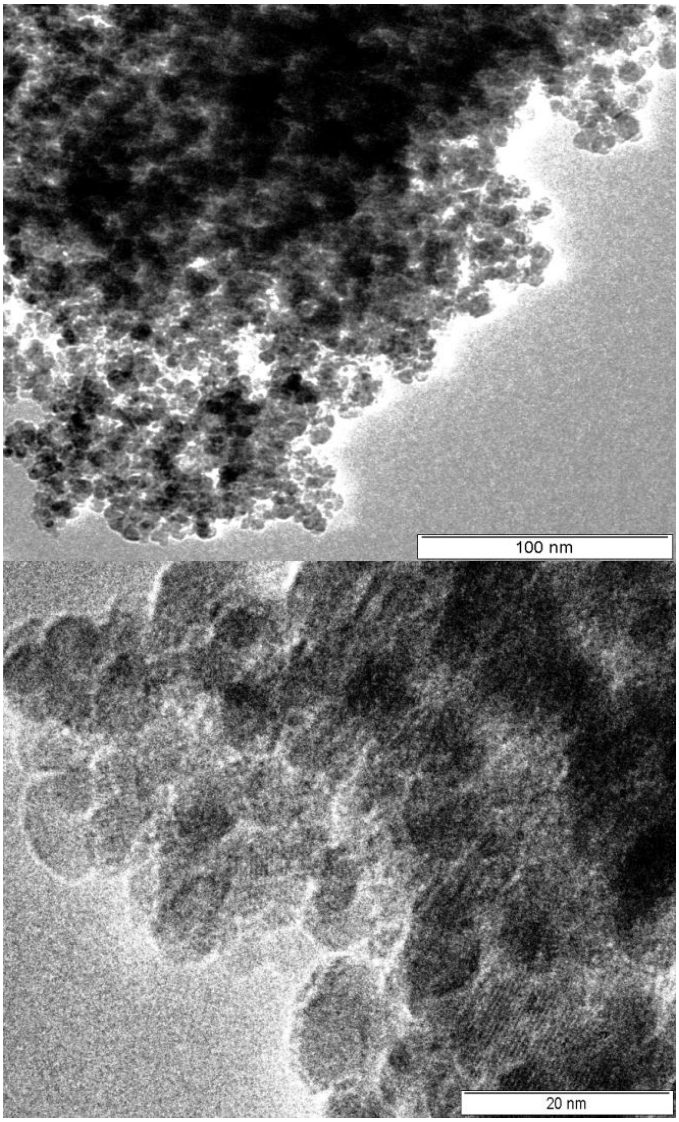

Figure 1(a-b). TEM of Nano-Nickel Zinc Ferrite

The TEM images for the ferrites have been shown in Figures 1(a) and 1(b). The morphology of the nano particles resembles a sphere with a size ranging between 10 to 15 nm [28]. FESEM images

for the particles as shown in Figure 2, represent the powder in the form of agglomerates of sizes ranging between 1to10 μm. The aggregation of particles is due to the magnetic attraction between the particles [29].

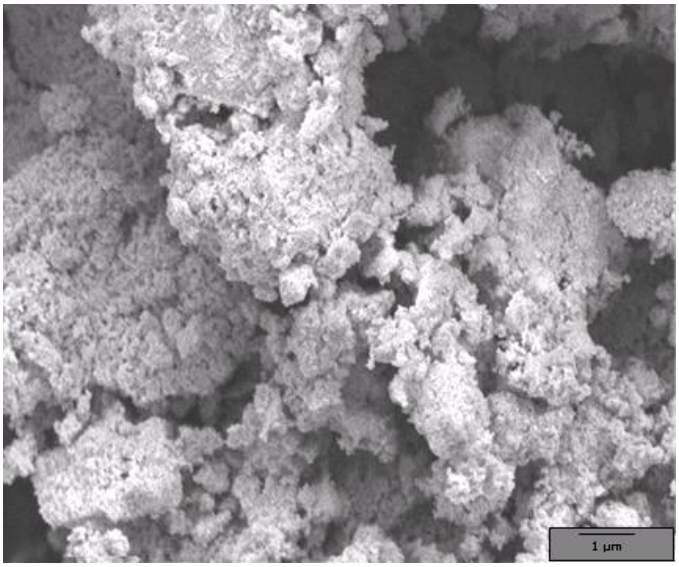

Figure 2. FESEM of Nickel Zinc Ferrite showing agglomerated of nanoparticles

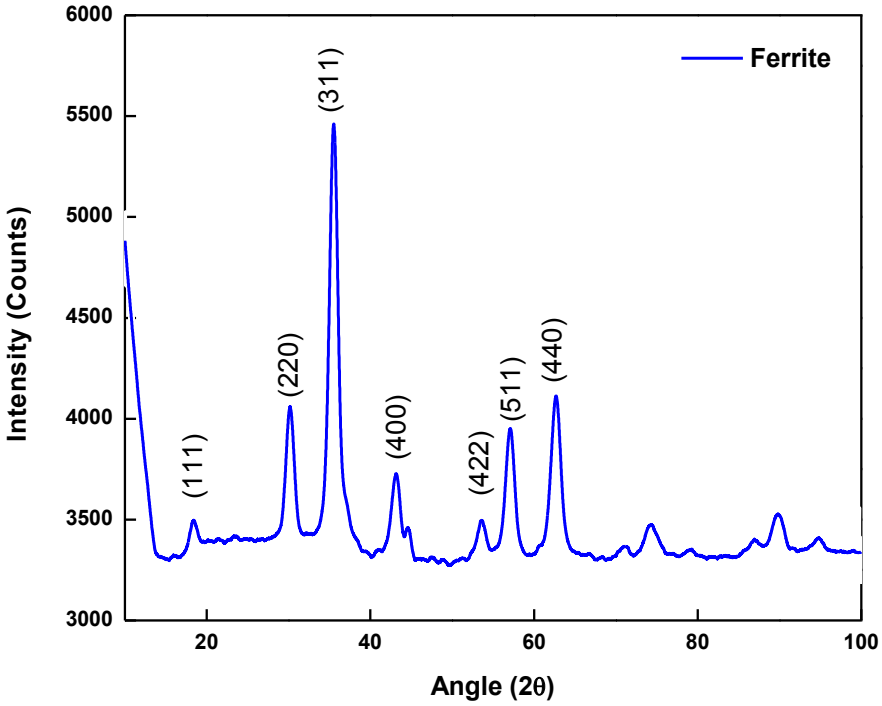

Figure 3. X-ray diffraction study of Nickel Zinc Ferrite

X-ray diffraction pattern obtained for nickel zinc ferrites has been shown in Figure 3 (JCPDS No.08-0234). The particle size as determined using Scherrer formula was found to be 12 nm which is in close range as calculated from TEM.

The analysis showed the presence of cubic spinal structure of the ferrites with a lattice parameter of 8.4A° and corresponding planes of (111), (220), (311), (400), (422), (511), and (440), representing the ferrite lattice [6].

3.1. Electrochemical characterization

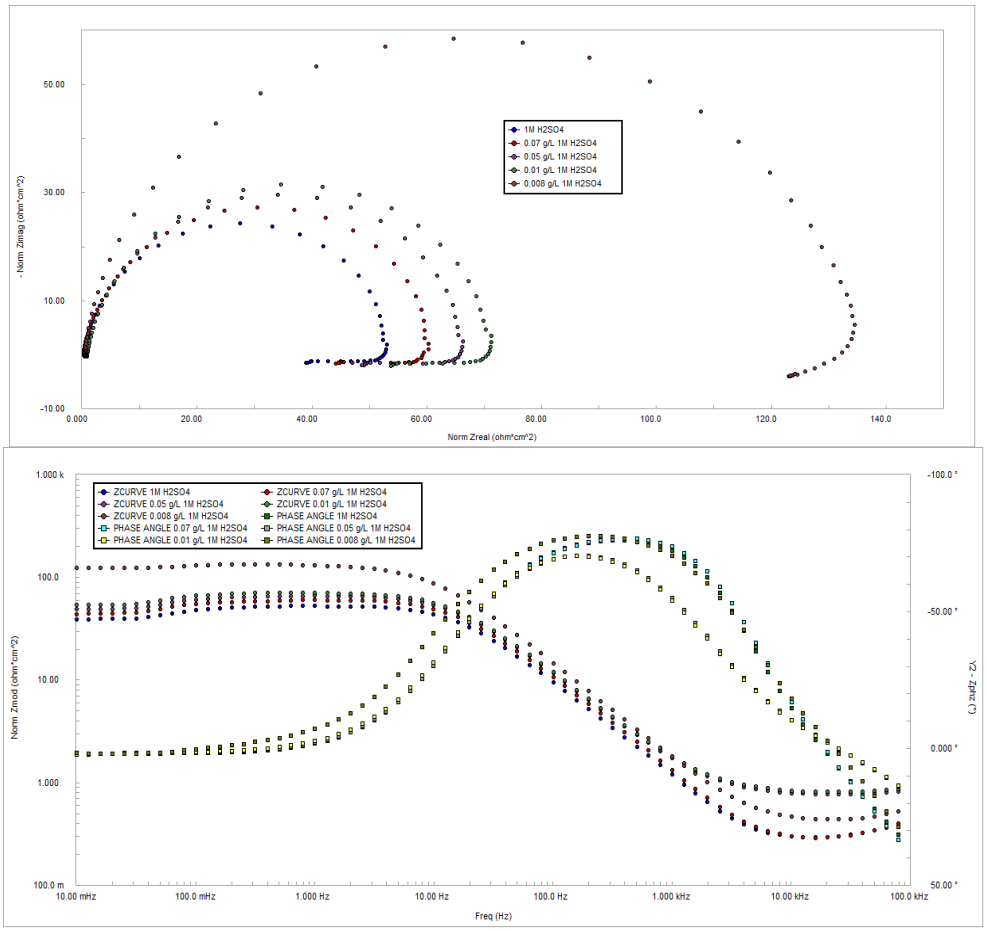

Figure 4. Impedance plots (Nyquist & Bode) for varying concentrations of Nickel Zinc Ferrite in 1M H_2SO_4 at 2 hours

Figures 4 and 5 present the EIS Nyquist and Bode curves respectively for varying ferrite concentrations in 1M H_2SO_4. At both 2 and 5 hours of immersion, the alloy shows a one time constant impedance response for all concentrations of ferrites. This behaviour can be easily noticed in the phase angle Bode curves as a single hump for the one time constant phase response. The inhibition efficencies of the different ferrities concentrations increase with time as noticed in Table 1. This indicates the stability of the protective ferrite film formed over the alloy surface.

Figure 6 represents the mono-phasic circuit model used to fit EIS data. This circuit model simulates the structure of a barrier coating over the electrode surface and is composed of R_s, the solution resistance and R_{ct} and CPE, the resistance and capacitance of the barrier layer.

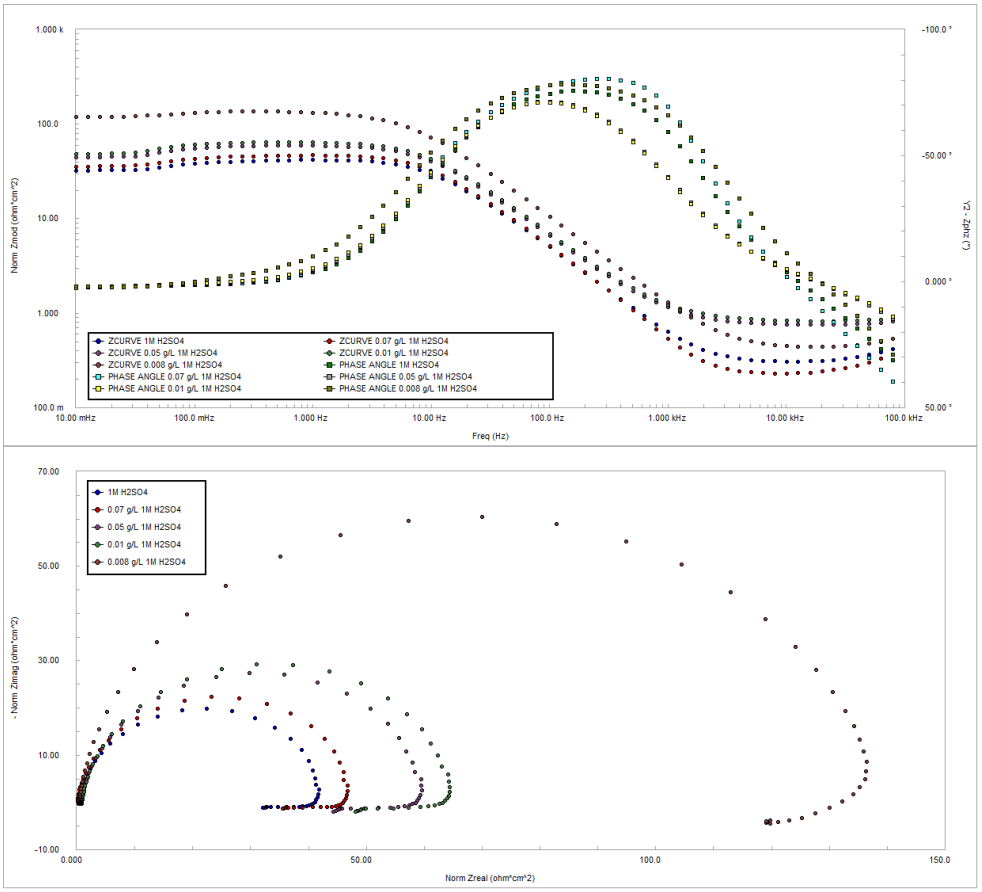

Figure 5. Impedance plots (Nyquist & Bode) for varying concentrations of Nickel Zinc Ferrite in 1M H_2SO_4 at 5 hours

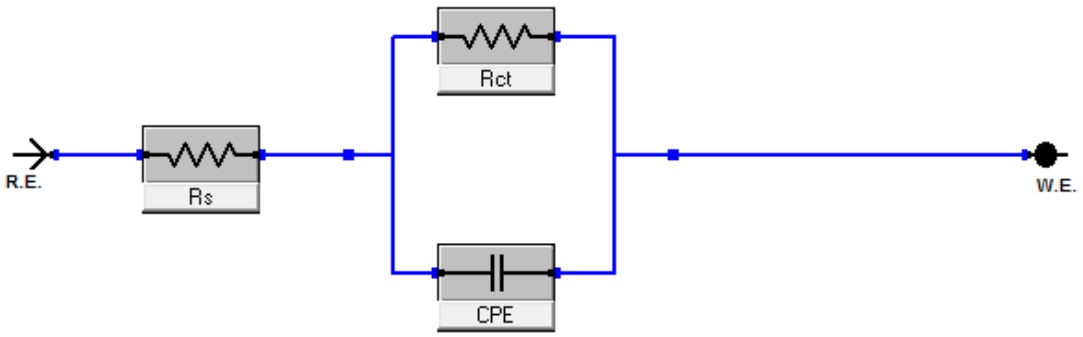

Figure 6. Circuit model used to fit the impedance plots

Assumption of a simple R_{ct} – C_{dl} is usually a poor approximation especially for systems showing depressed semicirlce behaviour. For the description of a frequency independent phase shift between the applied AC potential and its corresponding current response, a constant phase element (CPE) is used, where impedance of the CPE is given by,

$$Z\,(CPE) = [Q\,(j\omega)^n]^{-1} \qquad - 4$$

where, Q is the constant of CPE, ω is the angular frequency in rad s^{-1} and n is the exponential term which can vary between 1 for pure capacitance and 0 for a pure resistor [19, 30-32]. n is a measure of surface in homogeneity; the lower is its value, the higher is the surface roughening of the metal/alloy [32].

Table 1. Impedance parameters derived from circuit modeling.

At 2 hours of immersion

Concentration of Nickel Zinc Ferrite (g/L)	R_S	R_{ct}	IE %	CPE	α
0.0084	0.44	128.6	63.57	$1.44 * 10^{-4}$	0.956
0.016	0.82	63.75	26.52	$1.92 * 10^{-4}$	0.938
0.05	0.782	58.74	20.25	$1.89 * 10^{-4}$	0.942
0.07	0.297	53.23	12.00	$1.63 * 10^{-4}$	0.987
1M H_2SO_4	0.298	46.84	-	$1.81 * 10^{-4}$	0.981

At 5 hours of immersion

Concentration of Nickel Zinc Ferrite (g/L)	R_S	R_{ct}	IE%	CPE	α
0.0084	0.44	128.9	72.64	$1.99 * 10^{-4}$	0.959
0.016	0.839	57.52	38.69	$3.16 * 10^{-4}$	0.950
0.05	0.769	53.01	33.48	$3.33 * 10^{-4}$	0.955
0.07	0.235	41.66	15.36	$2.89 * 10^{-4}$	0.973
1M H_2SO_4	0.931	35.26	-	$4.65 * 10^{-4}$	0.961

R_s, R_{ct}, and CPE values derived from the impedance plots have been tabulated in Table 1.

R_{ct} value is the lowest for pure acid, representing its low resistance to conduction of charge/electrons and thereby allowing easy flow of electrons over the metal surface resulting in oxidation of iron to the ferrous state (equation 5). According to the Butler-Volmer concept involving polarization with charge transfer kinetics, higher R_{ct} restricts the movement of charges and prevents the various reactions occurring during the corrosion process. It increases from 46.8 Ω cm^2 for pure acid to 128.6 Ω cm^2 for the lowest concentration of ferrite.

Moreover, the R_{ct} value is the highest for the lowest concentration of ferrite and decreases as the concentration of ferrite increases, suggesting greater corrosion inhibition effect at low ferrites concentrations. This result is economically relevant to industry and thus proposes ferrites as efficient corrosion inhibitors for industrial applications.

The potentiodynamic polarization curve for varying concentrations of ferrites in 1 M H_2SO_4 has been presented in Figure 7. The corrosion rate for the alloy in 1M H_2SO_4 is close to 244 mpy compared to 51 mpy at the lowest concentration of ferrites. The potentiodynamic data is in agreement with the corrosion parameters obtained from the impedance plots and has been shown in Table 2.

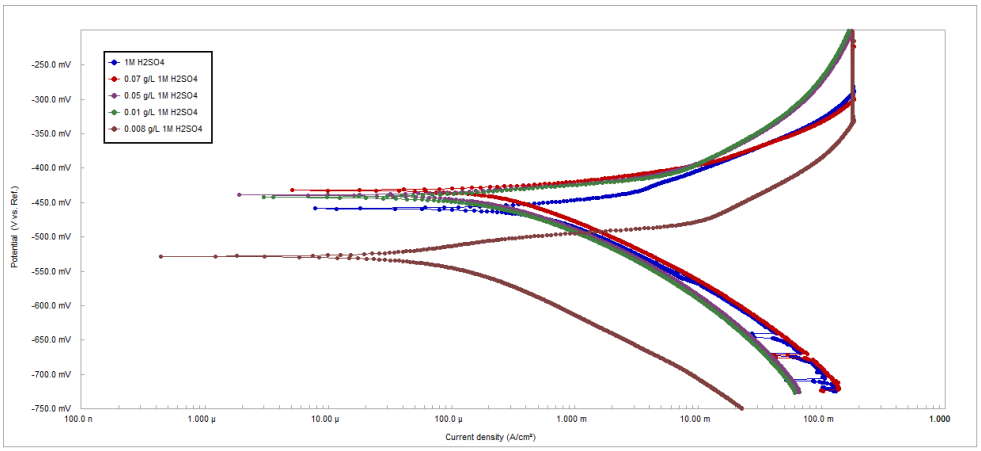

Figure 7. Potentiodynamic plots for varying concentrations of Nickel Zinc Ferrite in 1M H_2SO_4 at 5 hours

Table 2. Potentiodynamic parameters obtained from polarization curves at 5 hours.

Concentration of Nickel Zinc Ferritie in 1M H_2SO_4 (g/L)	I_{corr} (A/cm^2)	E_{corr} (mV)	Corrosion Rate (mpy)
0.008	$1.11 * 10^{-4}$	-528.50	50.91
0.01	$3.19 * 10^{-4}$	-442.2	161.7
0.05	$3.64 * 10^{-4}$	-439.0	166.3
0.07	$4.01 * 10^{-4}$	-432.1	183.4
1M	$5.31 * 10^{-4}$	-458.6	244.0

The lower corrosion rate at the lowest ferrite concentration makes it suitable to be used in industrial application economically and efficiently. The different ferrites concentrations follow the corrosion inhibition efficiency as follows; 0.008 > 0.01 > 0.05 > 0.07 > 1M sulphuric acid, thus lesser the amount higher is the inhibition advantage.

3.2. Surface characterization:

The inhibition of iron corrosion in the presence of sulphuric acid owing to the formation of ferrous sulphate ($FeSO_4$) has been proposed by several authors [33].

The various reactions taking part in the surface phenomena are summarized below[34];

$$Fe \rightarrow Fe^{2+} + 2\bar{e} \quad \text{(anodic)} \qquad -5$$

$$2H^{+} + 2\bar{e} \rightarrow H_2 \quad \text{(cathodic)} \qquad -6$$

$$Fe + H_2SO_4 \rightarrow FeSO_4 + H_2 \quad \text{(overall reaction)} \qquad -7$$

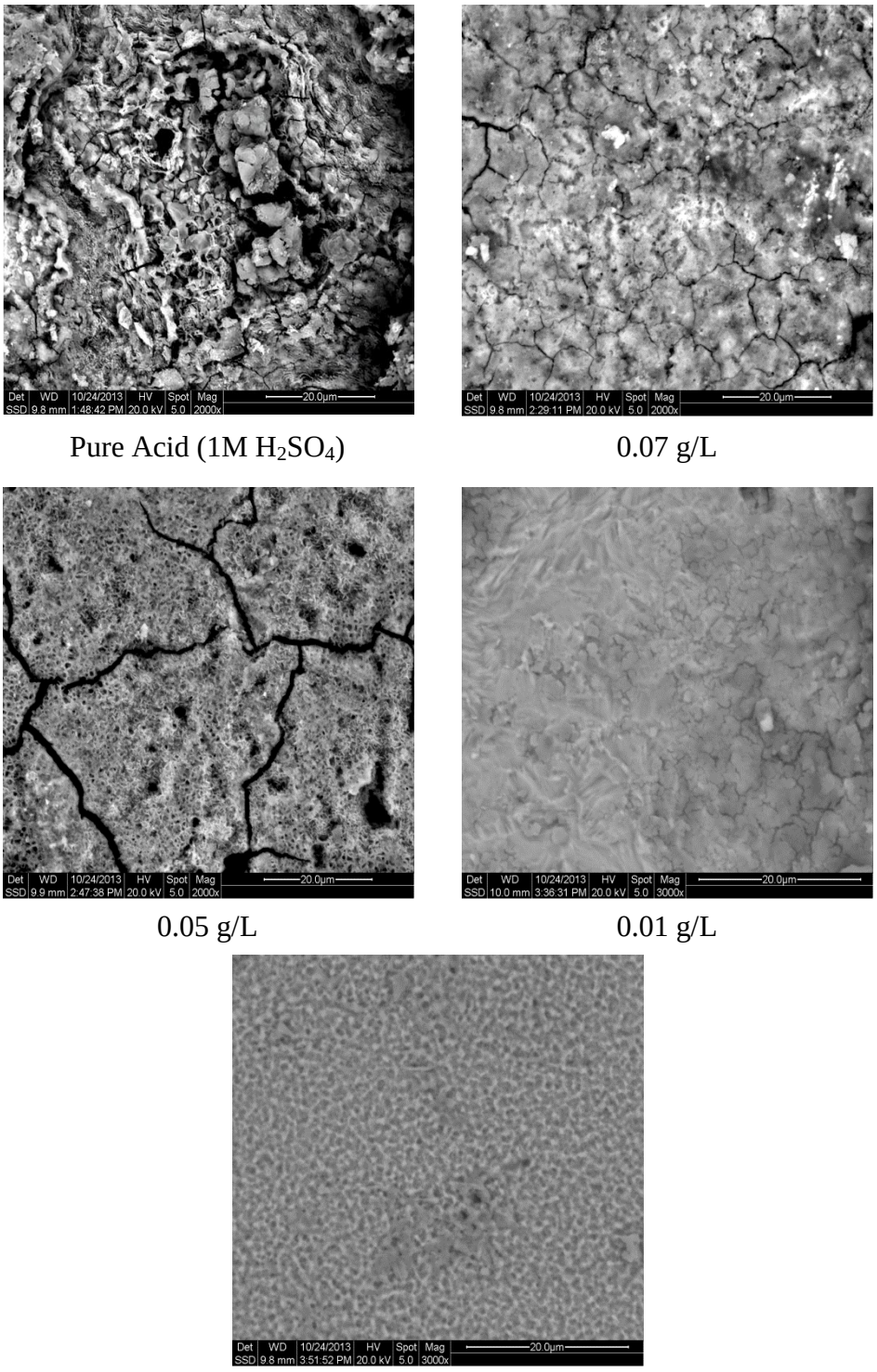

Pure Acid (1M H_2SO_4) 0.07 g/L

0.05 g/L 0.01 g/L

0.008 g/L

Figure 8. ESEM images of steel coupons for varying concentrations of Nickel Zinc Ferrite in 1M H_2SO_4

ESEM coupled with EDS was used to comprehend the surface morphology and elemental composition of the corrosion products over the metal coupons exposed to varying concentrations of ferrites and pure acid and has been shown in Figures 8a-8e.

It was observed that each concentration revealed a peculiar image with the greatest surface damage over the pure acid and the least damage with minimal ferrite concentration in acid solution. The ferrites form a coherent and homogeneous layer on the metal surface and thus inhibit corrosion. EDS analysis over the metal samples revealed two regions; lighter region and darker region. The lighter region corresponds to the surface rich in corrosion products comprising of sulphur and oxygen as shown in Figure 9a. The darker region represents the deeper areas with lesser concentrations of sulphur and oxygen compared to the lighter region. The presence of iron, sulfur and oxygen were found in general with a little amount of zinc and nickel in Figure 9b, present as various compounds in ferrite over the surface. The presence of zinc and nickel cations can be attributed to surface adsorption of ferrites over the metal surface [20, 33].

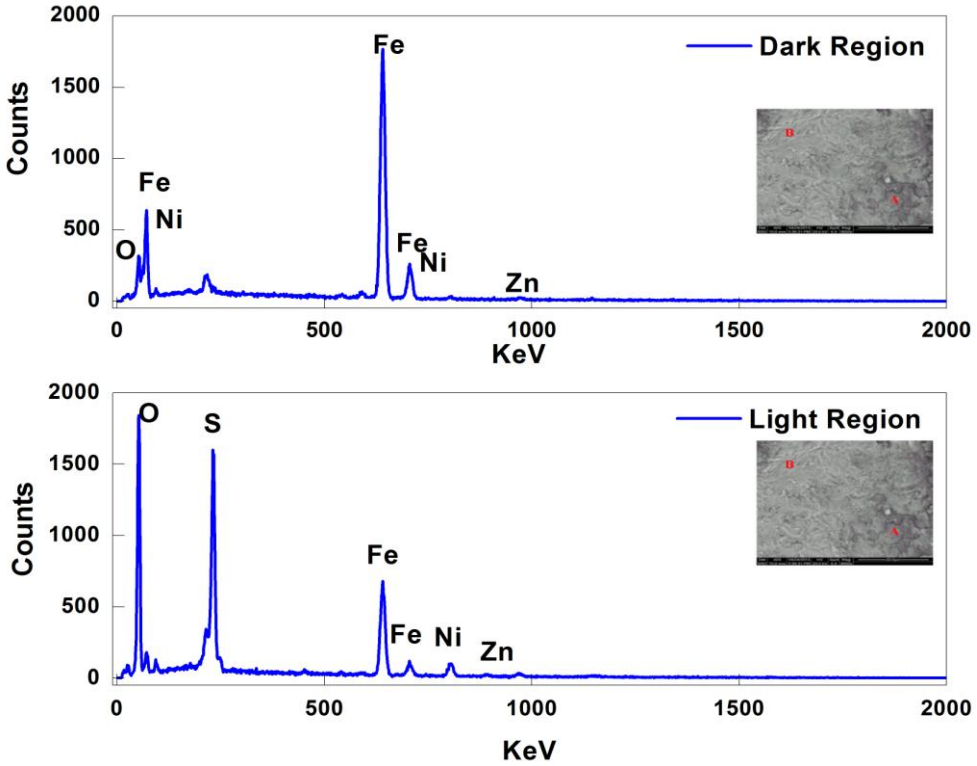

Figure 9. Energy dispersive spectroscopy (EDS) of steel samples surface after testing in 0.01 g/L (a) Light Region (b) Dark Region

Figure 10, shows the X-ray diffraction pattern for the mixed phases present on the metal surface. X-ray diffraction was used to differentiate the various mixed phases by comparing obtained data with JCPDS cards issued by ICDD [35]. Surface pattern over the pure steel coupon was also examined. The characteristic peaks of iron carbide and α-ferrite were observed in case of carbon steel surface at a $2\theta \sim 44°$ corresponding to (510) JCPDS 20-509 and a $2\theta \sim 82°$ corresponding to the (211) JCPDS 6-696 respectively. These two peaks were also observed in all the cases of corroded samples.

In case of 1M sulphuric acid not only the intrinsic carbon steel peaks, but also the peaks for the mixed phases of hydrous iron sulfate and iron sulfide were observed corresponding to 2θ ~ 41.5°($\bar{6}$12) and 2θ ~ 42.5°($\bar{1}$31) [36] respectively.

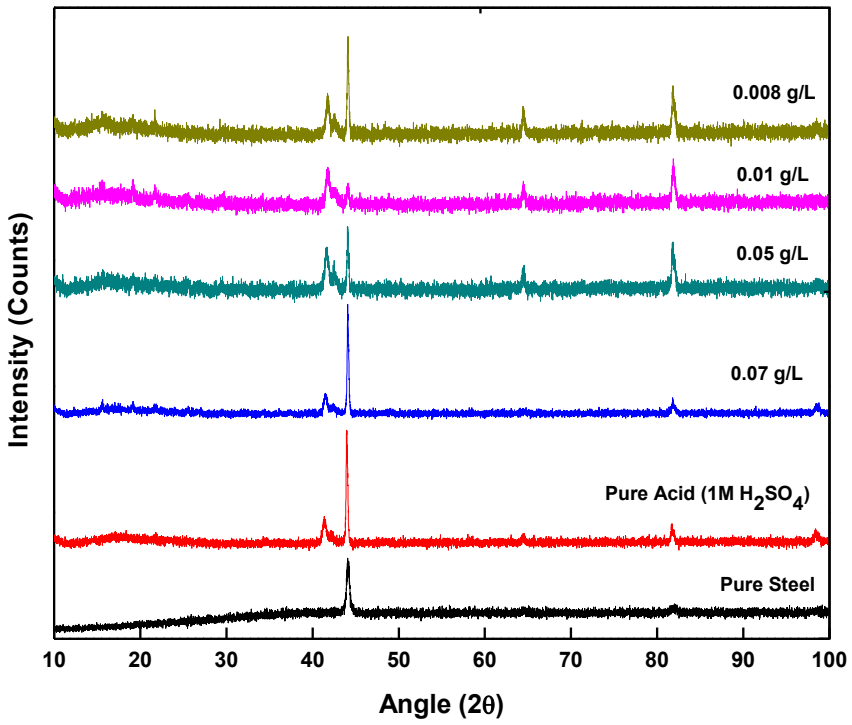

Figure 10. XRD pattern of surface

These peaks were also observed in the XRD patterns for varying concentrations of ferrites in acid. In those cases where ferrite inhibitor was used, mixed phases such as nickel sulfide 2θ ~ 15.5°(002) JCPDS 24-1021, 2θ ~19°(022), 2θ ~21.5°(040) JCPDS 24-1021, zinc sulfide 2θ ~ 29.5°(104), 2θ ~ 27°(100), 2θ ~ 34°(106) JCPDS 12-688 and iron sulfide 2θ ~ 25.5°(220) were observed.

The analysis confirms that adsorption of zinc and nickel occurs on the surface [19, 37] and react to form sulfides in the same manner as iron reacts to form sulfide or sulfate. This leads to the formation of a protective film and prevents corrosion in the presence of ferrite particles.

Figure 11 shows the FT-IR spectra for the different phases present over the metal surface. The characteristic band at ~1080 cm^{-1} represents the formation of sulfates [38] and is not observed over the steel sample. The characteristic peaks at ~1089 in pure sulphuric acid, 1088.8 in 0.07 g/L, 1090 in 0.05 g/L, 1086 in 0.01 g/L, and 1080 cm^{-1} in 0.008 g/L represent sulfates in various acid concentrations. Small proportions of characteristic iron oxide [39] peak at ~1090 cm^{-1} were also observed. The band at 1635 cm^{-1} could be due to the presence of adsorbed water in corroded samples while this band does not appear on the pure steel sample[39]. Magnetite (Fe_2O_3) peaks were also observed at ~600 cm^{-1} in few samples.

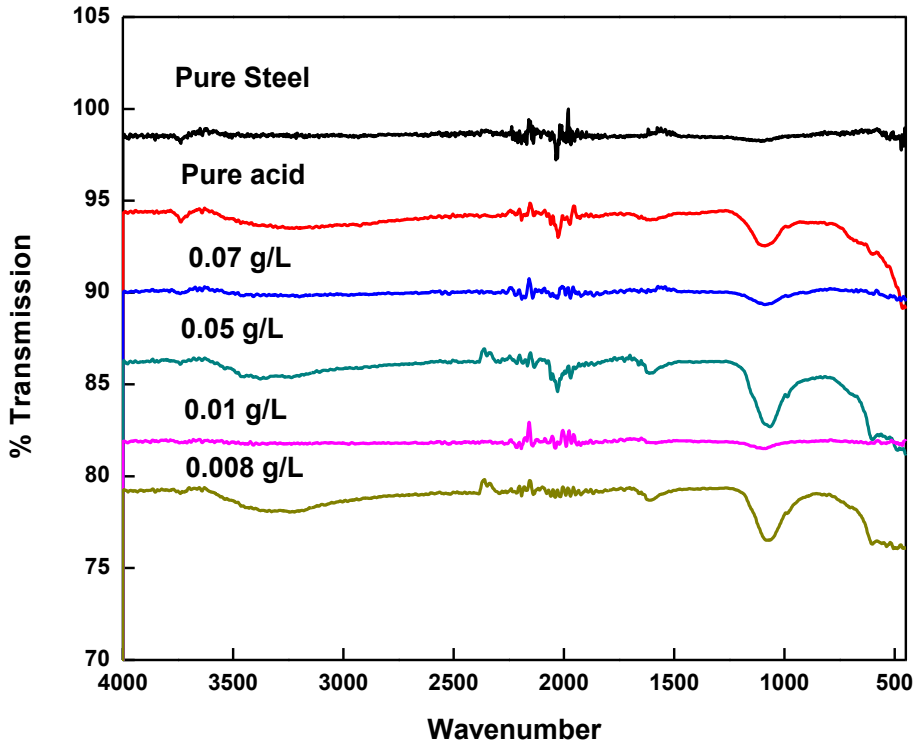

Figure 11. FT-IR spectra for varying concentration of Nickel Zinc Ferrite in 1M sulphuric acid

4. CONCLUSIONS

Anti corrosion behavior of Nickel Zinc Ferrite is well recognized and could be of significant help in corrosion inhibition in various industrial processes.

The API 5L X80 steel investigated in sulphuric acid with varying concentrations of ferrites exhibit considerable decrease in corrosion rate compared to the one without ferrites.

The lowest concentration of ferrites exhibit higher corrosion inhibition compared to the others and hence it can be used in minimal quantities economically and efficiently.

The use of such a small concentration of inhibitor as a filler in various polymeric materials may act as a starting point in developing self healing and corrosion resistant protective coatings.

References

1. S. M. Bhola, G. Singh and B. Mishra, *Int J Electrochem Sci*, 8 (2013)
2. S. Malhotra and G. Singh, *Surf Eng*, 21 (2005)
3. S. M. Bhola, F. M. Alabbas, R. Bhola, J. R. Spear, B. Mishra, D. L. Olson and A. E. Kakpovbia, *Eng Fail Anal*, 36 (2014)
4. V. S. Saji, *Recent Pat Corros Sci*, 2 (2010)
5. E. A. Noor, *Int J Electrochem Sci*, 2 (2007)
6. M. S. Al-Qubaisi, A. Rasedee, M. H. Flaifel, S. H. Ahmad, S. Hussein-Al-Ali, M. Z. Hussein, E. E. Eid, Z. Zainal, M. Saeed and M. Ilowefah, *Int J Nanomedicine*, 8 (2013)
7. A. L. Ferna´ndez and L. d. Pablo, *Pigm Resin Technol*, 31 (2002)

8. P. A. Sørensen, S. Kiil, K. Dam Johansen and C. E. Weinell, *J Coating Technol Res,* 6 (2009)
9. A. Miszczyk and K. Darowicki, *Anti-Corros Methods Mater,* 58 (2011)
10. V. Mittal, A. U. Chaudhry and M. I. Khan, *J Dispersion Sci Technol,* 33 (2011)
11. U. R. Evans, Metallic Corrosion, Passivity and Protection in Arnold & Co. London (1937)
12. A. Amirudin, C. Barreau, R. Hellouin and D. Thierry, *Prog Org Coat,* 25 (1995)
13. M. J. Pryor, *J Electrochem Soc*, 101 (1954)
14. J. Brodinova, J. Stejskalb and A. Kalendova´, *J Solid State Electr,* 68 (2007)
15. K. H. Wu, C. M. Chao, C. H. Liu and T. C. Chang, *Corros Sci,* 49 (2007)
16. M. H. Wahdan and G. K. Gomma, *Mater Chem Phys,* 47 (1997)
17. S. Licht, R. Tenne, H. Flaisher and J. Manassen, *J Electrochem Soc,* 133 (1986)
18. D. M. Dražić and L. Ž. Vorkapić, *Corros Sci*, 18 (1978)
19. S. Sathiyanarayanan, C. Jeyaprabha, S. Muralidharan and G. Venkatachari, *Appl Surf Sci,* 252 (2006)
20. V. S. Saji and J. Thomas, *Current Sci,* 92 (2007)
21. X. Shi, T. A. Nguyen, Z. Suo, Y. Liu and R. Avci, *Surf Coat Tech,* 204 (2009)
22. I. M. Zin, *Mater Sci,* 36 (2000)
23. ASTM-G61-86, *Standard Test Method for Conducting Cyclic Potentiodynamic Polarization Measurements for Localized Corrosion Susceptibility of Iron-, Nickel-, or Cobalt-Based Alloys*, ASTM International
24. ASTM-G3-89, *Standard Practice for Conventions Applicable to Electrochemical Measurements in Corrosion Testing*, ASTM International
25. A. G5., *Standard Reference Test Method for Making Potentiostatic and Potentiodynamic Anodic Polarization Measurements*, ASTM International West Conshohoken, PA
26. R. Bhola, S. M. Bhola, B. Mishra and D. L. Olson, *Res Lett Phys Chem,* 2009 (2009)
27. R. Bhola, C. Chandra, F. M. Alabbas, S. Kundu, B. Mishra and D. L. Olson, *Int J Corros,* 2013 (2013)
28. R. Misra, A. Kale, B. Kooi and J. T. M. De Hosson, *Mater Sci Tech,* 19 (2003)
29. S. Zahi, *J Electromagnet Anal App,* 2 (2010)
30. S. M. Bhola, R. Bhola, B. Mishra and D. L. Olson, *J Mater Sci: Mater in Med,* 22 (2011)
31. C. Hsu and F. Mansfeld, *Corros,* 57 (2001)
32. S. Chongdar, G. Gunasekaran and P. Kumar, *Electrochim Acta,* 50 (2005)
33. F. Ferrer, T. Faure, J. Goudiakas and E. Andrès, *Corros Sci,* 44 (2002)
34. Z. Panossian, N. L. d. Almeida, R. M. F. d. Sousa, G. d. S. Pimenta and L. B. S. Marques, *Corros Sci,* 58 (2012)
35. B. D. Cullity and J. W. Weymouth, *Am J Phys,* 25 (1957)
36. H. E. Swanson, H. F. McMurdie, M. C. Morris and E. H. Evans, *Standard X-ray Diffraction Powder Patterns: Section 8. Data for 81 Substances.*, Institute for Materials Research National Bureau of Standards
37. I. Singh and M. Singh, *Corros,* 43 (1987)
38. F. A. Miller and C. H. Wilkins, *Anal Chem,* 24 (1952)
39. J. A. Jaén, J. Iglesias and C. Hernández, *Int J Corros,* 2012 (2012)